Low temperature pyrolysis of thin film composite polyphosphazene membranes for hot gas separation

Radmanesh, F.; Tena, A.; Sudhölter, E. J.R.; Benes, N. E.

DOI
10.1016/j.mtnano.2023.100379

Publication date
2023

Document Version
Final published version

Published in
Materials Today Nano

Materials Today Nano 24 (2023) 100379

Contents lists available at ScienceDirect

Materials Today Nano

journal homepage: www.sciencedirect.com/journal/materials-today-nano

Low temperature pyrolysis of thin film composite polyphosphazene membranes for hot gas separation

F. Radmanesh [a], A. Tena [b,c], E.J.R. Sudhölter [a,d], N.E. Benes [a,*]

[a] Membrane Science and Technology Cluster, Faculty of Science and Technology, MESA+ Institute for Nanotechnology, University of Twente, P.O. Box 217, 7500 AE, Enschede, the Netherlands
[b] The European Membrane Institute Twente, Faculty of Science and Technology, University of Twente, P.O. Box 217, 7500 AE, Enschede, the Netherlands
[c] SMAP, UA-UVA_CSIC, Research Unit Associated to CSIC, Faculty of Science, University of Valladolid, Paseo Belén 11, E-47011, Valladolid, Spain
[d] Organic Materials & Interfaces, Department of Chemical Engineering, Faculty of Applied Sciences, Delft University of Technology, 2629 HZ, Delft, the Netherlands

ARTICLE INFO

Keywords:
Thin film composite membranes
Gas barriers
Interfacial polymerization
Carbon Molecular Sieve
Cyclic Phosphazene

ABSTRACT

Highly selective thin-film composite membranes for hot hydrogen sieving are prepared via the pyrolysis of thin cyclomatric polyphenoxy phosphazene films that are prepared via a non-conventional interfacial polymerization of hexachlorocyclotriphosphazene with 1,3,5-trihydroxybenzene or *m*-dihydroxybenzene. The presence of the cyclic phosphazene ring within the weakly branched polymer films gives rise to a distinct thermal degradation evolution, with an onset temperature of around 200 °C. For the trihydroxybenzene derived material, the hydrogen permselectivity of the films shows a maximum pyrolysis temperature of around 450 °C. At this temperature a compact atomic structure is obtained that comprises mostly disordered carbon and accommodates P–O–C and P–O–P bonds. During thermal treatment, these films reveal molecular sieving with permselectivities exceeding 100 for H_2/N_2, H_2/CH_4, and H_2/CO_2, and a hydrogen permeance of 2×10^{-10} to 1.5×10^{-8} mol/m^2/s/Pa (0.6-44.8GPU), at 200 °C. At ambient temperatures, thin films are very effective barriers for small gas molecules. Because of the inexpensive facile synthesis and low- temperature pyrolysis, the polyphosphazene films have the potential for use in high-temperature industrial gas separations, as well as for use as barriers such as liners in high- pressure hydrogen storage vessels at ambient temperature.

1. Introduction

Establishing a hydrogen-based economy has widespread momentum in many climate strategies [1–3]. This will require, amongst others, industrial-scale technology for molecular separation of hydrogen from other gases, such as CO, CO_2, and CH_4 [3–5]. Membrane-based separation technology can contribute to this [5–7]. Carbon molecular sieve (CMS) membranes have been reported to exhibit good performance in selective H_2 separation processes [5–7]. CMS materials are fabricated via pyrolysis, under an inert atmosphere, of polymer networks comprising condensed hexagonal rings without a three-dimensional crystalline order [8]. The resulting materials have sub-nanometer pores with sizes and shapes that depend strongly on the type of polymer precursors and the applied thermal treatment conditions. Polymers including polybenzimidzole (PBI), Matrimid®, cellulose, polypyrrole, and polyimide with intrinsic microporosity have been pyrolyzed to develop membranes containing the elements C, N, and F [5,8–11]. For example, Matrimid® pyrolyzed at 675 °C has a H_2/CO_2 permselectivity of 1.3 at room temperature [11], and polybenzimidzole (PBI) pyrolyzed at 900 °C has a H_2/CO_2 permselectivity of 80 at 150 °C [8]. Cellulose-based hollow fiber membranes pyrolyzed at 850 °C have H_2/CO_2 permselectivity of 83.9, H_2/N_2 permselectivity >800, and H_2/CH_4 selectivity >5700, at 130 °C [5]. CMS membranes can have a self-supporting asymmetric structure or can consist of a thin layer atop a porous ceramic or steel support. For the latter so-called Thin- film composite (TFC) membranes, preserving a continuous defect-free permselective thin film during pyrolysis is a challenge [12–15]. Richter et al., report a 125 nm thick carbon layer inside an asymmetric alumina tube through pyrolysis of a cross-linked unsaturated polyester, with H_2/CO_2 permselectivity of ~3 at 25 °C [12]. Another study reports alumina-supported CMS membranes via pyrolysis of phenol-formaldehyde resins at 500 °C, with permselectivities for H_2/CO_2 (~3), H_2/N_2 (~17), and H_2/CH_4 (~36.6), at 80 °C.

Recently, our group pioneered with a non-conventional interfacial

* Corresponding author.
E-mail address: n.e.benes@utwente.nl (N.E. Benes).

https://doi.org/10.1016/j.mtnano.2023.100379
Received 26 September 2022; Received in revised form 22 June 2023; Accepted 18 July 2023
Available online 24 July 2023

polymerization (IP) technique for the fabrication of ultrathin cyclomatrix polyphosphazene films [16]. Central in this method is the replacement of the aqueous phase with a DMSO/KOH solution. In this super base, the aromatic hydroxy compounds can be partly converted to highly soluble and nucleophilic aryloxide anions. This allows for the fast nucleophilic substitution of the Cl groups in the hexachlorocyclotriphosphazene (HCCP) that is dissolved in the non-polar cyclohexane phase. The obtained thin film polyphosphazene networks have tuneable gas permeance, ranging from gas-tight barriers to molecular sieves for hydrogen at temperatures well above 200 °C [16]. The thermal stability of the films is exceptional. In part, this is due to the strong Ar–O bonds between the organic bridges and the HCCP molecules; these bonds are stronger than the amide or ester bonds that are prevalent for IP-derived materials. In addition, the cyclic HCCP has inherent high thermal stability and heat resistance due to the symmetrically distributed P atoms and the unvarying N–P bond length resulting from the dπ-pπ hybrid orbital overlap [17]. The thermal decomposition of the HCCP ring is an endothermic process. In addition, HCCP has a high limiting oxygen index (minimum percentage of oxygen in a mixture of oxygen and nitrogen needed for flaming combustion), and when added as an additive to polymers, gives rise to cross-linked phosphorus oxynitride and carbonized aromatic networks in the solid phase [18–20]. The various phosphates formed in the combustion form non-volatile protective obstructions that impede the transport of oxygen and non-flammable combustion products, as well as the transport of heat. These properties make cyclomatrix polyphosphazene a popular non-halogenated additive for enhanced flame retardancy [19].

In our previous studies, we have demonstrated that the almost complete substitution of the Cl groups by diphenol bridges result in an abrupt thermal degradation behavior with a high onset temperature of ~400 °C [16]. In contrast, materials in which a limited number of the Cl groups are substituted by small aromatic hydroxyls exhibit a gradual thermal degradation, with an onset temperature of around ~250 °C [21]. This gradual degradation facilitates controlled pyrolysis at relatively mild conditions, resulting in thin films with final atomic compositions (many heteroatoms) and structures that are distinct from other CMS materials. Here, we explore the pyrolysis of moderately cross-linked cyclomatrix polyphosphazene membranes with various temperature trajectories under N_2 atmosphere.

2. Experimental

2.1. Materials

Phosphonitrilic chloride trimer (HCCP, 99%), 1,3,5-trihydroxybenzene (THB, ≥99%), *m*-dihydroxybenzene (MDHB, ≥99.9%), and dimethyl sulfoxide (DMSO, anhydrous, ≥99.9%) were supplied from Sigma-Aldrich. Cyclohexane (EMSURE for analysis), and potassium hydroxide (KOH, pellets extra pure) were obtained from Merk. Macroporous α-alumina discs with a diameter of 39 mm, a thickness of 2 mm, and a pore size of 80 nm were purchased from Pervatech B.V. and used as support.

2.2. Material fabrication

Free-standing polymer membrane layers and thin-film composite polymeric membranes were formed by interfacial polymerization of a 10 w/v% solution of the THB or MDHB, aromatic hydroxy compounds (AHC), in DMSO and KOH, super base [22], and a 3.5 w/v% HCCP solution in cyclohexane. The mol ratio of hydroxyl groups (monomers: KOH) is denoted *x* and was kept at 3.5:1. This hydroxyl ratio was chosen based on the earlier experiments and it is close to the minimum amount of KOH for making a free-standing layer. THB or MDHB is partly deprotonated by using KOH. Nucleophilic substitution takes place by the attack of the phenolate anions on the phosphor atoms of the HCCP rings, displacing the chlorine atoms. The formed networks are denoted THB-HCCP and MDHB-HCCP.

2.2.1. Synthesis of free-standing films

Free-standing films were prepared as follows: first, the AHC solutions were heated at 80 °C for 2.5 h. Next, the HCCP solution in cyclohexane was poured atop the AHC solution while still hot. The reaction happened as soon as the two solutions were brought into contact, and it was confirmed by visual observation of the formation of a thin layer. After 10 min, the formed thin film at the interface was collected, filtered, and washed with acetone, ethanol, and water and dried in a vacuum oven at 50 °C.

2.2.2. Preparation of thin-film composite membranes

The α-alumina discs were coated with a 3 μm thick γ-alumina (porosity of ~40% and pore size of 2–3 nm) based on the reported procedure [23]. The ceramic supports were heated to 80 °C for 2.5 h. After this, the support was impregnated with 5 ml of AHC solution in the oven at 80 °C for 10 min. Next, it was taken out, and its surface was dried by applying a rubber roller and an N_2 gun. Then, the support was submerged into 5 ml of HCCP solution at ambient temperature. After 10 min reaction time, the solution was discarded from the surface, and the membranes were rinsed with ethanol to remove any residual reactant. The membrane was kept under a fume hood overnight and then dried in a vacuum oven at 50 °C for a minimum of 24 h.

2.2.3. Thermal treatment

Thermal treatment was done in an STF (single zone furnace) 16/610 tubular furnace (Carbolite) equipped with an alumina working tube under N_2 atmosphere. The membrane was thermally treated according to the protocols given in Table 1. The final temperature was reached at a ramp rate of 2 °C/min. The furnace was evacuated and refilled with N_2 two times before treatment, followed by thermal treatment under an N_2 flow of 200 mL/min. The thermally treated samples are labeled as network's name-*xxx*, where *xxx* represents the final temperature (°C) used in the thermal treatment process.

2.3. Material characterization

A field emission-scanning electron microscope (FE-SEM, Zeiss MERLIN) was used to envision the thickness and morphology of the membranes. Samples were prepared by immersion into liquid nitrogen for 5 min before breaking them. For EDX analysis, all samples were dried and coated with a 5 nm Pt/Pd conductive layer using a sputter coater Quorum Q150T ES (Quorum Technologies, Ltd., UK) and was done at 10 kV with >1000 counts/s. Fourier transform infrared spectroscopy in attenuated total reflectance mode (FTIR-ATR, PerkinElmer Spectrum Two, USA) was used to characterize the powder product formed over 16 scans with a resolution of 4 cm^{-1} over a wavelength range of 400–4000 cm^{-1}. The elemental composition of synthesized powders was measured with X-Ray Fluorescence (XRF) (S8 Tiger, Bruker) and C,N elemental analysis (FLASH 2000 series analyzer). X-ray photoelectron spectroscopy (XPS) measurements were performed on PHI Quantes scanning XPS/HAXPES microprobe using a monochromatic Al Kα source (1486.6 eV). The binding energies of the benzene ring (from the aromatic

Table 1
Overview of the used protocols and their label for thermal treatment of the membranes.

Name	Treatment
Network-200	10 h at 200 °C
Network -250	Network-200 + 10 h at 250 °C
Network-300	Network -250 + 10 h at 300 °C
Network-350	Network-300 + 10 h at 350 °C
Network-450	Network-350 + 10 h at 450 °C
Network-550	Network-450 + 10 h at 550 °C
Network-650	Network-550 + 10 h at 650 °C

hydroxy compounds) were fixed in the carbon elemental fit of the prepared powders. Thermogravimetric Analysis (TGA, STA 449 F3 Jupiler®, Netzsch) in combination with mass spectrometry (MS, QMS 403 D Aeolos MS, Netzsch) was used to evaluate the thermal stability of the membranes. A fixed amount of sample (10 mg) was heated on a heating stage under an inert nitrogen atmosphere at a heating rate of 10 °C/min.

2.4. Membrane performance

Single gas permeance measurements were carried out using a dead-end mode setup (Inspector Poseidon, Convergence). The single gas permeance of He, N_2, CH_4, H_2, and CO_2 was measured at a transmembrane pressure of 2 bar within the temperature ranges from 50 to 250 °C. The gas permeation data were recorded for each gas by mass flow meters when it reached a steady state. The lower detection limit of the setup was 10^{-10} mol/m^2/s/Pa for an applied transmembrane pressure of 2 bar using the minimum detectable flow of the mass flow meters.

Permselectivity was calculated as the ratio of the respective permeances. The experiments were performed at least twice, and the reported results are the average of the obtained values.

3. Result and discussion

Fig. 1A gives a schematic representation of the preparation of polyphosphazene networks on top of ceramic supports using the approach reported in the earlier report [21]. Fig. 1B and C show top views of the thin film composites obtained after pyrolysis at various temperatures under an inert atmosphere. The color of samples changes with temperature. Both the MDHB and THB-derived samples have an orange color after treatment at 200 °C, and change to black after treatment at 450 °C. After treatment at 550 °C, the color of the MDHB-HCCP sample becomes white, indicating that the layer is gone. For THB-HCCP, the dark color after 550 °C is an evidence that a layer is still present; after 650 °C, this layer is also gone. The SEM micrographs in Fig. 1D and E show the cross-sections of the samples treated at 450 °C and reveal the presence of thin layers, even after exposure to these high temperatures. The thicknesses of the layers, ~30 nm, are comparable to those of the untreated samples [21]. This is distinct from other CMS membranes that generally reveal substantial changes in dimensions and mass [5,8].

Fig. 2A and B depict FTIR spectra of the monomers and the free-standing layers before and after pyrolysis. The spectra for the untreated free-standing films confirm network formation during the IP process. The broad peak in the range of 1100–1250 cm^{-1} belongs to the asymmetric P═N stretching vibration of HCCP [24], and the peak

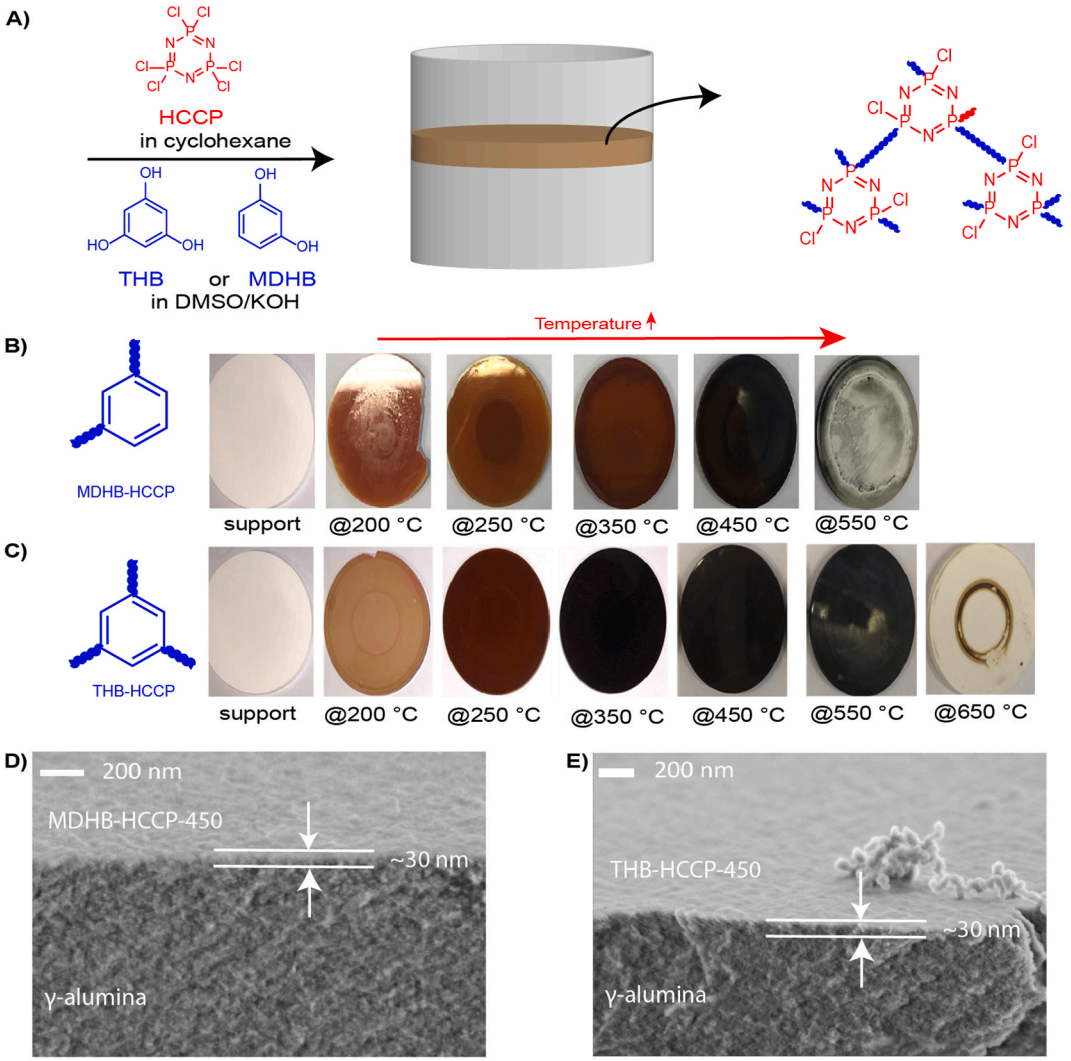

Fig. 1. (A) Schematic representation of MDHB-HCCP and THB-HCCP membrane preparation. (B) Effect of thermal treatment on the appearance of MDHB-HCCP membranes. (C) Effect of thermal treatment on the appearance of THB-HCCP membranes. (D) FE-SEM picture of MDHB-HCCP-450 membrane. (E) FE-SEM picture of THB-HCCP-450 membrane. The dark rings in the centers of the samples are a consequence of the sealing rings that were used in permeation experiments.

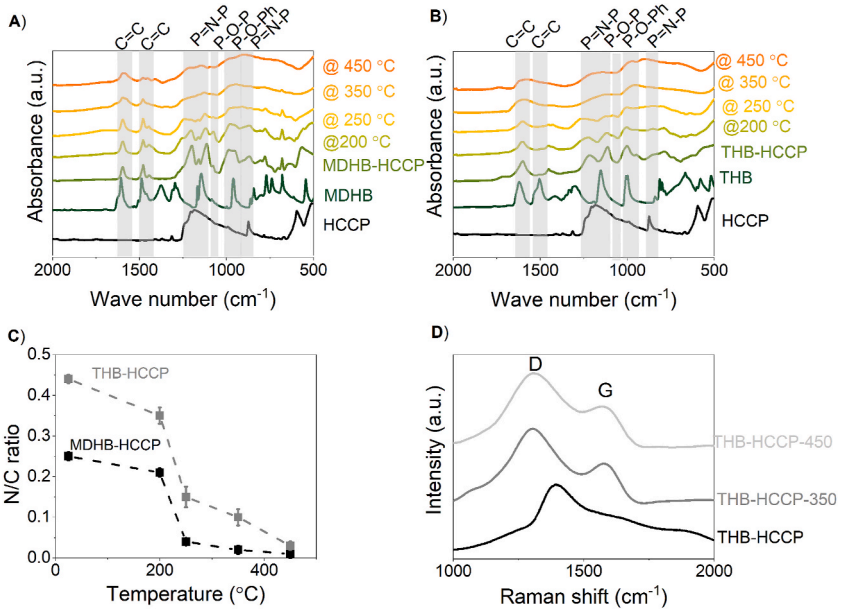

Fig. 2. FTIR spectra of monomers and formed networks before and after heat treatment (A)MDHB-HCCP. (B) THB-HCCP. (C) Effect of thermal treatment temperature on the N/C ratio in the synthesized powders see also Table S1. (D) Raman spectra of THB-HCCP, THB-HCCP-350, and THB-HCCP-450 with D and G bands representing disordered carbon and highly oriented graphitic carbon, respectively.

around 873 cm^{-1} is ascribed to the symmetric P═N stretching vibration [24]. Covalent connection is confirmed by the peaks at 950 cm^{-1} and 1003 cm^{-1} that are assigned to the stretching vibration of Ar-O-P [25]. After treating the samples at 200 °C, their spectra become less discrete. The Ar-O-P peaks intensify for both networks, implying further cross-linking of the networks. There is an overall increase in the intensity of adsorption in the range 1079 cm^{-1} that can be attributed to the formation of P–O bonds, such as P–O–P and other phosphates [26–28]. This becomes progressively more pronounced after treatment at higher temperatures. After treatment at 350°, peaks at 1400 and 1600 cm^{-1}, corresponding to the C═C bond, become broad and increases. This suggests that at these temperatures, both materials consist of phosphorus-rich carbonaceous structures [28].

EDX data in Table 2 and Table S1 confirm that, after treatment at 350 °C and 450 °C, the elemental composition of the materials comprises mainly carbon, oxygen, and phosphor. At these temperatures, most nitrogen is removed from the material. This is consistent with the decline in N/C ratio with temperature in Fig. 2C and Table S2, as determined from C,N elemental analysis. For both samples, the N/C ratio decreases slightly upon treatment at 200 °C, which is attributed to an increase in the extent of cross-linking at this temperature. This is shown by an increase in the P/Cl ratio observed by XRF (Table S3) upon treatment at 200 °C, indicating that the thermal treatment increases the connection from an average of 2 to an average of 4–5 organic bridges per HCCP core. Further cross-linking can originate from reactions between unreacted phenolates and P–Cl moieties and reactions between P–Cl and P–OH groups of hydrolyzed HCCP [29]. A further increase in the pyrolysis temperature from 200 to 250 °C causes a strong further decline in the N/C ratio due to the loss of N from the collapsing HCCP core [24,30]. This removal of nitrogen progresses further to 350 °C and 450 °C.

Table 2
EDX data, elemental concentrations for pyrolyzed THB-HCCP powders *what do the errors mean, in particular for the ratios.

	Elemental concentration(%)			
	THB-HCCP	THB-HCCP-200	THB-HCCP-350	THB-HCCP-450
C	41.5 ± 2.8	39.5 ± 1.1	54.8 ± 1.8	51.1 ± 0.6
N	14.2 ± 0.5	13.0 ± 2.3	3.0 ± 0.1	2.3 ± 0.3
O	27.9 ± 2.9	23.8 ± 2	31.8 ± 1.5	33.0 ± 1.1
P	9.2 ± 1.1	18.4 ± 3.8	9.3 ± 0.3	12.0 ± 1.1
S	0.8 ± 0.1	1.3 ± 0.3	0.6 ± 0.1	0.7 ± 0.1
Cl	3.8 ± 1.5	3.1 ± 1.3	0.1 ± 0	0.2 ± 0
K	2.6 ± 1.0	1.1 ± 0.3	0.4 ± 0.2	0.6 ± 0.1
C/N	2.9 ± 0.2	3 ± 0.5	18 ± 0.8	22 ± 2.7
P/N	0.6 ± 0.1	1.4 ± 0.4	3.1 ± 0.2	5.2 ± 0.8
P/C	0.1 ± 0	0.5 ± 0.1	0.2 ± 0	0.2 ± 0

The Raman spectra in Fig. 2D gives an indication of changes in the atomic order/disorder in THB-HCCP, before and after pyrolysis at temperatures of 350 °C and 450 °C [31]. The two broad peaks that appear at ~1310 and ~1580 cm^{-1} correspond to the *D* and *G* bands, respectively [18]. The *D* band is assigned to the A_{1g} in-plain breathing vibration mode of disordered graphitic carbon [5]. The *G* band is associated with the E_{2g} in-plain vibration mode of graphitic carbon with an sp^2 electronic configuration and associates with the degree of graphitization [32]. The ratio of the intensity of the two peaks (I_D/I_G, Fig. S1) is 3.9 for TPE-HCCP-350 and 3.7 for TPE-HCCP-450. The decrease indicates more ordering of carbon at higher temperatures [33]. The graphitic crystallite size, estimated from the Tuinstra−Koenig equation $L_a = 4.4\ I_G/I_D$ [34], is 1.13 nm for THB-HCCP-350 and 1.19 nm for THB-HCCP-450, confirming a slightly more defective graphitic carbon in TPE-HCCP-350 [8]. In addition, at 450 °C the values of both I_D and I_G are higher, confirming more graphitization at a higher temperature. These observations are in line with the decomposition of the P–N rings at 350 °C and 450 °C derived from EDX and C,N elemental analysis. This explains why pyrolysis in our materials already occurs at lower temperatures than for other polymers [35]. The relatively low pyrolysis temperatures result in I_D/I_G values exceeding 1, indicative of relatively disordered carbon [36]. This is in contrast to polyphosphazene carbonized at a high temperature of 950 °C [37,38].

The thermally induced collapse of the HCCP ring is also evident from the XPS data. In Fig. S2, the N1s spectrum of THB-HCCP reveals two peaks corresponding to nitrogen in the HCCP ring. For THB-HCCP-200, the position and surface area under these peaks is changed, which we attribute to an increased extent of cross-linking. A further increase of the temperature to 250 °C and higher results in a completely different spectrum, implying that the ring opening of HCCP takes place and nitrogen is no longer accommodated in the ring structure of HCCP. The P2p spectrum exhibited nearly identical curves at different processing

steps of samples, Fig. S3. In Fig. S4, the C1s spectrum of THB-HCCP-350 shows two pronounced peaks located around 284.7 eV and 286.3 eV, corresponding to C═C/C–C and C–O/C–N, respectively. The percentage of functional groups can be calculated based on the area under each fitted peak. With increasing the pyrolysis temperature to 450 °C, the ratio of unconvoluted peak area of (C–O/C–N) to (C═C/C–C) decreases, indicating the conversion of C–O/C–N to more C═C/C–C groups, graphite-like carbon [36,35]. We can conclude an increase in the degree of graphitization which is in line with Raman spectroscopy. Also, it confirmed the results of the high-resolution N1s XPS spectrum.

The thermal stability of prepared polyphosphazene networks was evaluated by TGA-MS under N_2 and the detailed data are shown in Fig. S5. The untreated networks exhibit a three-step weight loss between 50 and 600 °C [21]. The removal of the trapped solvents and enhancing the extent of cross-linking happens from room temperature to ~250 °C. The second stage, between 250 °C and 400 °C, is attributed to the collapsing of the HCCP ring and partially carbonization of the network. Above 400 °C, further decomposition of aromatic rings and carbonization occurs [24]. Additionally, Fig. S5 shows that increasing the pyrolysis temperature decreases the mass of remaining char at 600 °C and enhances the onset of degradation due to removing the unstable bonds.

Fig. 3 reveals the changes in the microstructure of THB-HCCP free-standing films upon pyrolysis. Prior to pyrolysis, a regular continuous film covers the ceramic support. This morphology is reported in only a few other studies, all of which are based on a single-solvent polymerization technique [24,39,40]. Heating the sample to 200 °C does not substantially change this morphology. Exposure to 350 °C results in a completely distinct structure. This is partly caused by graphitization, but it is also due to the soft intumescent characteristics of the polyphosphazene in which materials swell when exposed to fire or heat to form a porous foamed mass. Pyrolysis leads to the formation of PO_x and phosphoric acid derivatives. These derivatives can react with carbon bonds to form P–O–C and P–O–P complexes [18]. Another study considers the formation of cross-linked phosphorus oxynitride and carbonized aromatic networks during combustion [19,20]. Increasing the temperature to 450 °C further affects the structure of the layer. The thermal degradation of the material creates a layer that can inhibit the transport of gaseous products, and shields part of the material from heat and air [18,19]. Fig. S6 shows the digital photos of the THB-HCCP-200 and THB-HCCP-450 powders from top and side views. The structure of THB-HCCP changes from flakes to porous structures after raising the treatment temperature from 200 °C to 450 °C. It confirms that at 450 °C the materials are indeed soft intumescent, and the size of the powder increases during thermal treatment.

The changes in the structure and morphology of the thin- film composites affect their permselective properties. The gas separation performances of the prepared membranes were tested with pure He, H_2, CO_2, N_2, and CH_4 at a temperature between 50 and 200 °C and at a transmembrane pressure of 2 bar. Fig. 4A and B presents the effects of pyrolysis temperature on the performance of MDHB-HCCP at 200 °C. For the MDHB-HCCP films, the exposure to higher temperatures results in a monotonous increase in the permeance of hydrogen at 200 °C, combined with an almost complete loss in permselectivity of hydrogen over nitrogen of methane. This observed trade-off suggests that pyrolysis leads to defects in the thin film. At a pyrolysis temperature of 450 °C, the surface color of the sample is still black, as can be seen in Fig. 1, but the permeances are comparable to those of the ceramic supports.

For THB-HCCP membranes, another behavior is observed, Fig. 4C and D. The permeance of hydrogen at 200 °C shows a substantial increase when the sample is thermally treated at 250 °C instead of 200 °C. This increase in permeance is accompanied by an increase in permselectivity of hydrogen over nitrogen or methane. The treatment at 250 °C causes enhanced cross-linking within the polymer network, enhancing its rigidity and changing the size and the shape of the free volume elements that it contains [41]. As a result, the diffusion mobility of hydrogen in the network becomes more significant. This is substantiated by the lower activation energy of the hydrogen permeance (Fig. S7), indicating the reduction in energy barriers for diffusion of hydrogen molecules. For the larger molecules, nitrogen and methane, this effect is less and an enhancement in permeance is less pronounced [41]. The hydrogen permeance and its activation energy, are comparable to those of very tight polybenzimidazole membranes at 39 bar 200 °C [42]. An increase in pyrolysis temperature to 300 °C does not significantly affect the permeance of hydrogen, while the activation energy reduces further. This can be explained by a lower amount of slightly larger free-volume elements. When the pyrolysis is performed at 350 °C, the activation energy is further reduced, but the permeance of 200 °C hot hydrogen does not significantly increase. This is attributed to the graphitization of part of the material, reducing the number of pathways that are available for diffusive transport. This is even more pronounced for a pyrolysis temperature of 450 °C, where the lowest H_2 permeance is observed. This can be attributed to the large extent of graphitization observed with Raman for this temperature as well as the formation of a barrier layer as a result of the intumescent characteristics of the polyphosphazene which

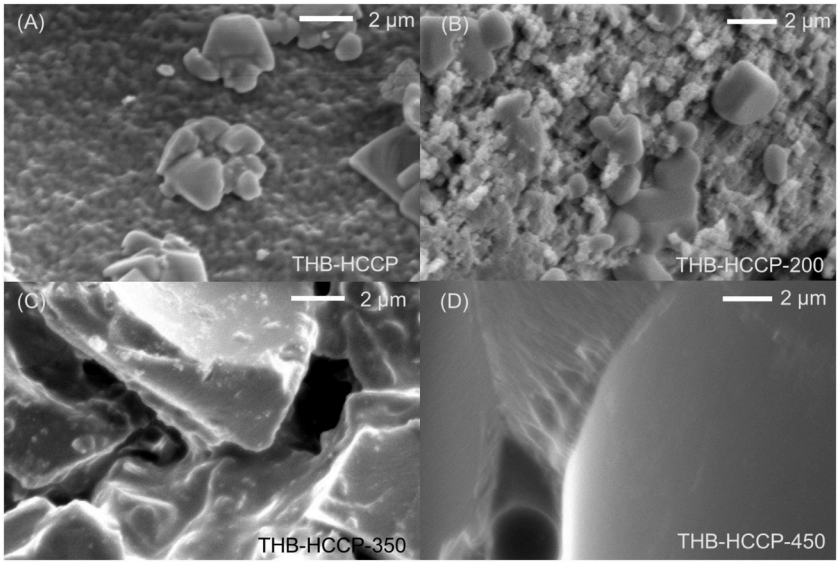

Fig. 3. SEM images of prepared powders. (A) THB-HCCP, (B) THB-HCCP-200, (C) THB-HCCP-350, and (D) THB-HCCP-450.

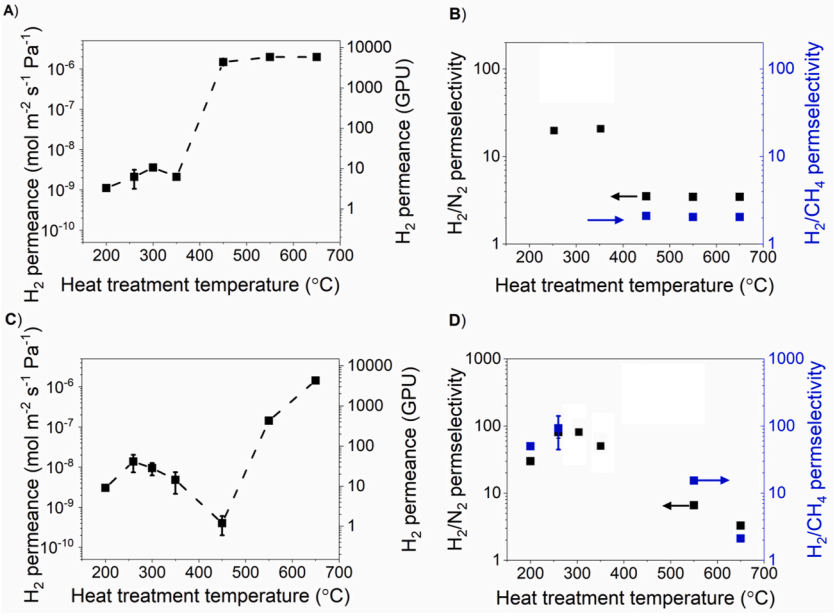

Fig. 4. Effect of pyrolysis temperature on the performance of MDHB-HCCP membranes at 200 °C (A) H_2 permeance, (B) H_2/N_2 and H_2/CH_4 permselectivity. Effect of the pyrolysis temperature on the performance of THB-HCCP membranes at 200 °C (C) H_2 permeance and ,(D) H_2/N_2 and H_2/CH_4 permselectivity. The calculated H_2/N_2 and H_2/CH_4 permselectivities for MDHB-HCCP-250. MDHB-HCCP-350, THB-HCCP-300, and THB-HCCP-350, are based on the considering the N_2 and CH_4 permeance as detection limit of the set up (1×10^{-10} mol/m^2/s/Pa) since those permeances were below the detection limit of the setup.

inhibits the transport of gas molecules. For this film, the highest permselectivity is observed, where the permeances of nitrogen and methane are below the detection limit of the setup. Pyrolysis at temperatures of 550 °C and higher results in a strong decrease in permselectivities, due to the formation of defects.

Because of the positive values of the activation energy for transport, the permeances of the gases reduce when their temperatures are lower. The result is that, at ambient temperature, the thin THB-HCCP-450 films are very good barriers for small gases, including hydrogen.

The H_2/CO_2 permselectivity of THB-HCCP is compared with that of other carbonized membranes including carbon hollow fiber (CHFM) [5], carbonized polyimide [43], carbonized polyester [12], carbonized polybezimidazole [8] at temperatures above 130 °C in a Robeson plot (Fig. 5). For THB-HCCP-250 and THB-HCCP-350, the CO_2 permeance is measured by the setup and it is below its detection limit and for permselectivity calculation, CO_2 permeance is assumed to be 1×10^{-10} as the detection limit of set- up. The THB-HCCP-250 and THB-HCCP-350 show similar H_2/CO_2 permselectivity compared to the other studies. In addition, the low permeability is compensated by the low thickness that can be achieved by the IP technique. Considering the separation performance for H_2/CO_2, H_2/CH_4 , and H_2/N_2, the thermally treated TPE-HCCP-250 and TPE-HCCP-350 can be suitable for H_2 purification on industrial scales.

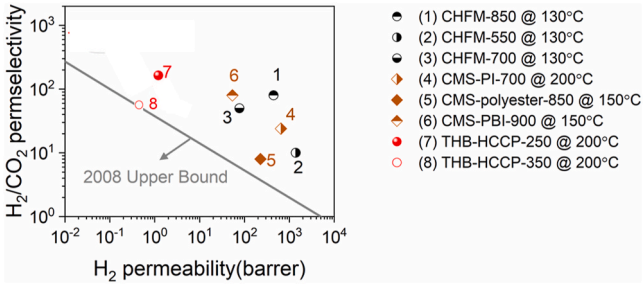

Fig. 5. Comparison of the H_2/CO_2 gas performance of the prepared membranes with state-of-the-art H_2/CO_2 carbonized and inorganic membrane materials tested in the temperature range of 130–200 °C. For THB-HCCP-250 and THB-HCCP-350, the CO_2 permeance is assumed to be 1×10^{-10} mol/m^2/s/Pa as the detection limit of set up. The H_2/CO_2 line is drawn based on the 2008 Robeson upper bound.

4. Conclusions

Pyrolysis of ultra-thin (~30 nm) cyclomatrix polyphosphazene membranes is used to tailor their gas separation performance. The thin-film composites are prepared by interfacial polymerization between a small aromatic hydrocarbon (in dimethyl sulfoxide with potassium hydroxide) and hexachlorocyclotriphosphazene in cyclohexane, followed by pyrolysis at temperatures between 200 and 650 °C. A combination of characterization techniques reveal that the onset of carbonization is as low as ~350 °C. The low pyrolysis temperatures, as compared to those employed in other membrane carbonization studies', result from the distinct thermal degradation of the phosphazene ring. For 1,3,5-trihydroxybenzene based polyphosphazene, pyrolysis at 450 °C gives the lowest observed hydrogen permeance of 200 °C. This is due to the unique hybrid material that is formed during pyrolysis, combining ordered and disordered graphitized structures and accommodating P–O–P and P–O–C bonds. Hydrogen permeance at 200 °C is of the order of 2×10^{-10} mol/m^2/s/Pa, the thin- film composites have very low gas permeance, that makes them potential barriers for small gas molecules including hydrogen at ambient temperature. For 1,3,5-trihydroxybenzene based polyphosphazene, heat treatment at 250 °C gives a hydrogen permeance of 1.5×10^{-8} at 200 °C and at least 100 higher as compared to permeance of nitrogen, methane, and carbon monoxide which makes the treated polyphosphazene membranes promising for use in high-temperature applications.

Credit author statement

Farzaneh Radmanesh: Conceptualization, Visualization, Data curation, Validation, Investigation, Methodology, Writing - original draft.

Alberto Tena: Methodology, Conceptualization, Writing - Review & Editing.

Ernst J.R. Sudhölter: Supervision, Supervision, Writing - Review & Editing.

Nieck E. Benes: Funding acquisition, Supervision, Conceptualization, Supervision, Writing - Review & Editing.

Declaration of competing interest

The authors declare that they have no known competing financial interests or personal relationships that could have appeared to influence

the work reported in this paper.

Data availability

Data will be made available on request.

Acknowledgments

This work is part of the GENESIS project and the authors acknowledge the financial support from the European Union's Horizon 2020 Research and Innovation Program under the Grant Agreement No. 760899.

Appendix A. Supplementary data

Supplementary data to this article can be found online at https://doi.org/10.1016/j.mtnano.2023.100379.

References

[1] A. Midilli, H. Kucuk, M.E. Topal, U. Akbulut, I. Dincer, A comprehensive review on hydrogen production from coal gasification: challenges and Opportunities, Int. J. Hydrogen Energy 46 (2021) 25385–25412, https://doi.org/10.1016/j.ijhydene.2021.05.088.

[2] H. Lin, E. Van Wagner, B.D. Freeman, L.G. Toy, R.P. Gupta, Plasticization-enhanced hydrogen purification using polymeric membranes, Science 311 (2006) 639–642, https://doi.org/10.1126/science.1118079.

[3] M. Noussan, P.P. Raimondi, R. Scita, M. Hafner, The role of green and blue hydrogen in the energy transition—a technological and geopolitical perspective, Sustainability 13 (2020) 298, https://doi.org/10.3390/su13010298.

[4] H.W. Kim, H.W. Yoon, S.-M. Yoon, B.M. Yoo, B.K. Ahn, Y.H. Cho, H.J. Shin, H. Yang, U. Paik, S. Kwon, J.-Y. Choi, H.B. Park, Selective gas transport through few-layered graphene and graphene oxide membranes, Science 342 (2013) 91–95, https://doi.org/10.1126/science.1236098.

[5] L. Lei, F. Pan, A. Lindbråthen, X. Zhang, M. Hillestad, Y. Nie, L. Bai, X. He, M. D. Guiver, Carbon hollow fiber membranes for a molecular sieve with precise-cutoff ultramicropores for superior hydrogen separation, Nat. Commun. 12 (2021), https://doi.org/10.1038/s41467-020-20628-9.

[6] C. Zhang, W.J. Koros, Ultraselective carbon molecular sieve membranes with tailored synergistic sorption selective properties, Adv. Mater. 29 (2017), 1701631, https://doi.org/10.1002/adma.201701631.

[7] W. Qiu, J. Vaughn, G. Liu, L. Xu, M. Brayden, M. Martinez, T. Fitzgibbons, G. Wenz, W.J. Koros, Hyperaging tuning of a carbon molecular-sieve hollow fiber membrane with extraordinary gas-separation performance and stability, Angew. Chem. Int. Ed. 58 (2019) 11700–11703, https://doi.org/10.1002/anie.201904913.

[8] M. Omidvar, H. Nguyen, Liang Huang, C.M. Doherty, A.J. Hill, C.M. Stafford, X. Feng, M.T. Swihart, H. Lin, Unexpectedly strong size-sieving ability in carbonized polybenzimidazole for membrane H 2/CO 2 separation, ACS Appl. Mater. Interfaces 11 (2019) 47365–47372, https://doi.org/10.1021/acsami.9b16966.

[9] W. Ogieglo, T. Puspasari, M.K. Hota, N. Wehbe, H.N. Alshareef, I. Pinnau, Nanohybrid thin-film composite carbon molecular sieve membranes, Mater. Today Nano. 9 (2020), 100065, https://doi.org/10.1016/j.mtnano.2019.100065.

[10] J.W.F. To, J. He, J. Mei, R. Haghpanah, Z. Chen, T. Kurosawa, S. Chen, W.-G. Bae, L. Pan, J.B.-H. Tok, J. Wilcox, Z. Bao, Hierarchical N-doped carbon as CO 2 adsorbent with high CO 2 selectivity from rationally designed polypyrrole precursor, J. Am. Chem. Soc. 138 (2016) 1001–1009, https://doi.org/10.1021/jacs.5b11955.

[11] M. Rungta, G.B. Wenz, C. Zhang, L. Xu, W. Qiu, J.S. Adams, W.J. Koros, Carbon molecular sieve structure development and membrane performance relationships, Carbon N. Y. 115 (2017) 237–248, https://doi.org/10.1016/j.carbon.2017.01.015.

[12] H. Richter, H. Voss, N. Kaltenborn, S. Kämnitz, A. Wollbrink, A. Feldhoff, J. Caro, S. Roitsch, I. Voigt, High-flux carbon molecular sieve membranes for gas separation, Angew. Chem. Int. Ed. 56 (2017) 7760–7763, https://doi.org/10.1002/anie.201701851.

[13] M.L. Jue, Y. Ma, R.P. Lively, Streamlined fabrication of asymmetric carbon molecular sieve hollow fiber membranes, ACS Appl. Polym. Mater. 1 (2019) 1960–1964, https://doi.org/10.1021/acsapm.9b00567.

[14] M. Acharya, H.C. Foley, Spray-coating of nanoporous carbon membranes for air separation, J. Membr. Sci. 161 (1999) 1–5, https://doi.org/10.1016/S0376-7388(99)00173-8.

[15] L. Forster, C. D'Agostino, M.A. Llosa-Tanco, V. Spallina, C. Brencio, F. Gallucci, M. Lindley, S.J. Haigh, D.A. Pacheco-Tanaka, Tailoring pore structure and surface chemistry of microporous Alumina-Carbon Molecular Sieve Membranes (Al-CMSMs) by altering carbonization temperature for optimal gas separation performance: an investigation using low-field NMR relaxation measurements, Chem. Eng. J. 424 (2021), 129313, https://doi.org/10.1016/j.cej.2021.129313.

[16] F. Radmanesh, E.J.R. Sudhölter, A. Tena, M.G. Elshof, N.E. Benes, Thin film composite cyclomatrix poly(phenoxy)phosphazenes membranes for hot hydrogen separation, Adv. Mater. Interfac. 4 (2023), 2202077, https://doi.org/10.1002/admi.20220207.

[17] X. Zhou, S. Qiu, X. Mu, M. Zhou, W. Cai, L. Song, W. Xing, Y. Hu, Polyphosphazenes-based flame retardants: a review, Compos. B Eng. 202 (2020), 108397, https://doi.org/10.1016/j.compositesb.2020.108397.

[18] S. Qiu, Y. Zhou, X. Zhou, T. Zhang, C. Wang, R.K.K. Yuen, W. Hu, Y. Hu, Air-stable polyphosphazene-functionalized few-layer black phosphorene for flame retardancy of epoxy resins, Small 15 (2019), https://doi.org/10.1002/smll.201805175.

[19] S. Qiu, X. Wang, B. Yu, X. Feng, X. Mu, R.K.K. Yuen, Y. Hu, Flame-retardant-wrapped polyphosphazene nanotubes: a novel strategy for enhancing the flame retardancy and smoke toxicity suppression of epoxy resins, J. Hazard Mater. 325 (2017) 327–339, https://doi.org/10.1016/j.jhazmat.2016.11.057.

[20] S. Qiu, W. Xing, X. Feng, B. Yu, X. Mu, R.K.K. Yuen, Y. Hu, Self-standing cuprous oxide nanoparticles on silica@ polyphosphazene nanospheres: 3D nanostructure for enhancing the flame retardancy and toxic effluents elimination of epoxy resins via synergistic catalytic effect, Chem. Eng. J. 309 (2017) 802–814, https://doi.org/10.1016/j.cej.2016.10.100.

[21] F. Radmanesh, A. Tena, E.J.R. Sudhölter, M.A. Hempenius, N.E. Benes, Non-aqueous interfacial polymerization derived polyphosphazene films for sieving or blocking hydrogen gas, ACS Appl. Polym. Mater. 3 (2023) 1955–1964, https://doi.org/10.1021/acsapm.2c02022.

[22] A.S. Bobkov, N.M. Vitkovskaya, B.A. Trofimov, Cascade assembly of 4,5,6,7-tetrahydroindole from cyclohexanone oxime and acetylene in the KOH/DMSO superbase medium: a quantum chemical study, J. Org. Chem. 85 (2020) 6463–6470, https://doi.org/10.1021/acs.joc.0c00353.

[23] X. Wang, P. Karakiliç, X. Liu, M. Shan, A. Nijmeijer, L. Winnubst, J. Gascon, F. Kapteijn, One-pot synthesis of high-flux b -oriented MFI zeolite membranes for Xe recovery, ACS Appl. Mater. Interfaces 10 (2018) 33574–33580, https://doi.org/10.1021/acsami.8b12613.

[24] M. Zhang, Y. Li, C. Bai, X. Guo, J. Han, S. Hu, H. Jiang, W. Tan, S. Li, L. Ma, Synthesis of microporous covalent phosphazene-based frameworks for selective separation of uranium in highly acidic media based on size-matching effect, ACS Appl. Mater. Interfaces 10 (2018) 28936–28947, https://doi.org/10.1021/acsami.8b06842.

[25] G. Tang, X. Zeng, L. Hou, T. Song, S. Yin, B. Long, A. Ali, G.-J. Deng, Cross-linked ultrathin polyphosphazene-based nanosheet with promoted charge separation kinetics for efficient visible light photocatalytic CO2 reforming to CH4, Appl. Catal. B Environ. 306 (2022), 121090, https://doi.org/10.1016/j.apcatb.2022.121090.

[26] S.J. Maynard, T.R. Sharp, J.F. Haw, Thermal degradation chemistry of poly (diphenoxyphosphazene), Macromolecules 24 (1991) 2794–2799, https://doi.org/10.1021/ma00010a024.

[27] M. El Gouri, A. El Bachiri, S.E. Hegazi, M. Rafik, A. El Harfi, Thermal degradation of a reactive flame retardant based on cyclotriphosphazene and its blend with DGEBA epoxy resin, Polym. Degrad. Stabil. 94 (2009) 2101–2106, https://doi.org/10.1016/j.polymdegradstab.2009.08.009.

[28] H. Liu, X. Wang, D. Wu, Synthesis of a novel linear polyphosphazene-based epoxy resin and its application in halogen-free flame-resistant thermosetting systems, Polym. Degrad. Stabil. 118 (2015) 45–58, https://doi.org/10.1016/j.polymdegradstab.2015.04.009.

[29] Y.W. Chen-Yang, S.J. Cheng, B.D. Tsai, Preparation of the partially substituted (phenoxy)chlorocyclotriphosphazenes by phase-transfer catalysis, Ind. Eng. Chem. Res. 30 (1991) 1314–1319, https://doi.org/10.1021/ie00054a036.

[30] M. Lv, C. Yao, D. Yang, H. Zeng, Synthesis of a melamine-cyclotriphosphazene derivative and its application as flame retardant on cotton gauze, J. Appl. Polym. Sci. 133 (2016), https://doi.org/10.1002/app.43555.

[31] J. Fu, Y. Huang, Y. Pan, Y. Zhu, X. Huang, X. Tang, An attempt to prepare carbon nanotubes by carbonizing polyphosphazene nanotubes with high carbon content, Mater. Lett. 62 (2008) 4130–4133, https://doi.org/10.1016/j.matlet.2008.06.020.

[32] K.N. Kudin, B. Ozbas, H.C. Schniepp, R.K. Prud'homme, I.A. Aksay, R. Car, Raman spectra of graphite oxide and functionalized graphene sheets, Nano Lett. 8 (2008) 36–41, https://doi.org/10.1021/nl071822y.

[33] X. Chen, Y. Fan, L. Wu, L. Zhang, D. Guan, C. Ma, N. Li, Ultra-selective molecular-sieving gas separation membranes enabled by multi-covalent-crosslinking of microporous polymer blends, Nat. Commun. 12 (2021) 1–12, https://doi.org/10.1038/s41467-021-26379-5.

[34] A.C. Ferrari, D.M. Basko, Raman spectroscopy as a versatile tool for studying the properties of graphene, Nat. Nanotechnol. 8 (2013) 235–246, https://doi.org/10.1038/nnano.2013.46.

[35] K. Rhili, S. Chergui, A.S. ElDouhaibi, M. Siaj, Hexachlorocyclotriphosphazene functionalized graphene oxide as a highly efficient flame retardant, ACS Omega 6 (2021) 6252–6260, https://doi.org/10.1021/acsomega.0c05815.

[36] M. Gao, J. Fu, M. Wang, K. Wang, S. Wang, Z. Wang, Z. Chen, Q. Xu, A self-template and self-activation co-coupling green strategy to synthesize high surface area ternary-doped hollow carbon microspheres for high performance supercapacitors, J. Colloid Interface Sci. 524 (2018) 165–176, https://doi.org/10.1016/j.jcis.2018.04.027.

[37] X. Zhang, S. He, X. Wo, T. Han, J.A.N.N. Kambonde, J. Wu, X. Qiu, L. Zhao, Enhanced specific capacity and cycle stability of hybrid supercapacitors using carbonized polyphosphazene-based nanocomposites, Electrochim. Acta 397 (2021), 139297, https://doi.org/10.1016/j.electacta.2021.139297.

[38] J.G. Seong, J.C. Lewis, J.A. Matteson, E. Craddock, U. Martinez, H. Thakkar, A. D. Benavidez, K.A. Berchtold, R.P. Singh, Polybenzimidazole-derived carbon molecular sieve hollow fiber membranes with tailored oxygen selective transport, Carbon N. Y. 192 (2022) 71–83, https://doi.org/10.1016/j.carbon.2022.02.033.

[39] F. Yang, M. Qiu, Z. Miao, T. Zhang, S. Zhang, Z. Wu, N, P-codoped carbon film derived from phosphazenes and its printing integration with a polymer carpet via

"molecular welding" for flexible electronics, ACS Appl. Mater. Interfaces 13 (2021) 29894–29905, https://doi.org/10.1021/acsami.1c04010.

[40] R. Jiang, B. Deng, L. Pi, L. Hu, D. Chen, Y. Dou, X. Mao, D. Wang, Molten electrolyte-modulated electrosynthesis of multi-anion Mo-based lamellar nanohybrids derived from natural minerals for boosting hydrogen evolution, ACS Appl. Mater. Interfaces 12 (2020) 57870–57880, https://doi.org/10.1021/acsami.0c17137.

[41] R. Xu, L. Li, X. Jin, M. Hou, L. He, Y. Lu, C. Song, T. Wang, Thermal crosslinking of a novel membrane derived from phenolphthalein-based cardo poly(arylene ether ketone) to enhance CO2/CH4 separation performance and plasticization resistance, J. Membr. Sci. 586 (2019) 306–317, https://doi.org/10.1016/j.memsci.2019.05.084.

[42] L. Zhu, M.T. Swihart, H. Lin, Tightening polybenzimidazole (PBI) nanostructure via chemical cross-linking for membrane H 2/CO 2 separation, J. Mater. Chem. A. 5 (2017) 19914–19923, https://doi.org/10.1039/C7TA03874G.

[43] P.H.T. Ngamou, M.E. Ivanova, O. Guillon, W.A. Meulenberg, High-performance carbon molecular sieve membranes for hydrogen purification and pervaporation dehydration of organic solvents, J. Mater. Chem. A. 7 (2019) 7082–7091, https://doi.org/10.1039/C8TA09504C.